Role of cellulose nanocrystals on hysteretic sorption and deformation of nanocomposites

Mingyang Chen, Benoit Coasne, Dominique Derome, Jan Carmeliet

Role of cellulose nanocrystals on hysteretic sorption and deformation of nanocomposites

Mingyang Chen [1, *], Benoit Coasne [2], Dominique Derome [3] and Jan Carmeliet [1]

1. Chair of Building Physics, ETH Zurich, Switzerland

2 .Univ. Grenoble Alpes, CNRS, LIPhy, France

3. Department of Civil and Building Engineering, Université de Sherbrooke, Canada

*****Correspondence: minchen@ethz.ch

Abstract: A molecular model of an all-cellulose nanocomposite, with an amorphous cellulose matrix reinforced by cellulose nanocrystals, is built to study the role of cellulose nanocrystal (CN) as a nanofiller in the coupled behavior between sorption and deformation. We find two competitive mechanisms. The first mechanism is the reinforcing effect through CN-matrix mechanical interaction, which constrains the sorption-induced swelling of the matrix and results in a reduction of sorption amount and of hysteresis in both sorption and deformation. The second mechanism is the CN-water interaction, enhancing water sorption in the matrix at the CN-matrix interface, increasing the sorption-induced swelling of the matrix, and increasing the resulting hysteresis in sorption and deformation. The final gain/reduction in sorption, swelling and related hysteresis depends on which of the two effects prevails. These findings shed light on the tailoring of cellulose-based composites for applications involving sorption and deformation.

Keywords: *sorption; deformation; hysteresis; all-cellulose nanocomposite*

1. Introduction

Cellulose nanocrystal (CN) exhibits high stiffness and strength, high surface area and unique morphology (Habibi et al. 2010a; Mariano et al. 2014). These features, together with their great sustainability and biodegradability, make CN ideal candidate to improve the mechanical properties of various materials (Habibi et al. 2010b; Mariano et al. 2014; Blanco et al. 2018). In nature, CN serves as mechanical reinforcement in several biomaterials (Brown 1996, 2004; Anfara et al. 2002; Williamson et al. 2002). For instance, the stiffness and strength of wood cell wall mainly come from the reinforcing effect of the microfibrils composed of CN (Salmén 2004; Derome et al. 2012; Chen et al. 2019b) For man-made materials, CN is incorporated as reinforcement into a wide range of polymer matrices such as poly(caprolactone) (Habibi et al. 2008), poly(oxyethylene) (Azizi Samir et al. 2004) and starch-based polymers (Anglès and Dufresne 2001). It is also incorporated into cellulosic matrix to form the so-called all-cellulose composites (ACC) (Qi et al. 2009). Given the chemical homogeneity of ACC, the reinforcement–matrix interface forms strong bonding. In addition, ACC can be straightforwardly recycled as the reinforcement and matrix do not require separation. These advantages make ACC a promising biodegradable "green" composite (Nishino et al. 2004; Huber et al. 2012).

Cellulose being hydrophilic, the responses of CN-reinforced composites to moisture must be clearly understood and described. The interaction between composites and moisture is used as an asset for example in CN-reinforced composites developed for water purification (Yu et al. 2013; Karim et al. 2014; Liu et al. 2017; Rafieian et al. 2019). Biomaterials such as wood or man-made composites are in service commonly exposed to environmental moisture

conditions, leading to a change of hygromechanical behavior, eventually to degradation (Patera et al. 2016; Kafy et al. 2016). The amorphous polymeric matrix of composites has an open microstructure and water can be adsorbed into the matrix (Kulasinski et al. 2017). During sorption, water creates its own space by increasing the host porosity. In so doing, water sorption is accompanied by swelling which results in an intrinsic coupling between sorption and deformation, commonly referred to as sorption-induced deformation (Barkas 1939; Kulasinski et al. 2016; Chen et al. 2018, 2020) Further, sorption in nanoporous polymers displays a strong hysteresis in terms of moisture content versus relative humidity (RH), but hysteresis collapses in terms of moisture content versus strain (Patera et al. 2013; Chen et al. 2018). Also seen is a hysteresis in mechanical property versus moisture content, but not versus hydrogen bonds between polymeric chains (Chen et al. 2018). The presence of CN makes the coupling between hysteretic sorption and swelling even more complex as these nanocrystals may play multiple roles in the coupling physics. CN can influence water sorption: infrared spectroscopy shows that water molecules form clusters at the CN/matrix interface (Maréchal and Chanzy 2000; Hofstetter et al. 2006), indicating that the presence of CN yields hydrophilic interfaces within the composites. In addition, CN can have mechanical impact on the matrix. The effect of CN as a mechanical reinforcement has been extensively studied experimentally for different composite systems (Favier et al. 1995; Taylor 2002). These studies show that CN can improve the matrix both in terms of stiffness and strength and the improvement relies on a strongly bonded CN/matrix interface. The multiple roles played by CN can be competing. For instance, it has been observed experimentally that water uptake in CN-reinforced nanocomposites decreases monotonically with increasing CN content (Anglès and Dufresne 2000; de Mesquita et al. 2012; Mariano et al.

2014), while some other experiments show that this dependence is non-monotonic (Sanchez-Garcia and Lagaron 2010; Sánchez-García et al. 2010; Mariano et al. 2014). This suggests that CN enhance sorption in some circumstances while hinder sorption in others. Moreover, sorption and swelling of CN-based composites are found to be dependent on moisture history (Derome et al. 2011; Safari and van de Ven 2016), i.e., hysteresis is present in the sorption and strain isotherms. For a better understanding of the dependence of composite properties on CN, the effects of CN on coupling of sorption and deformation and the related hysteresis have to be clarified.

Water sorption in nanocomposites can be modeled by molecular simulations, including molecular dynamics (MD) and Monte Carlo (MC) simulations (Charlier and Mazeau 2012; Mazeau and Charlier 2012; Kulasinski et al. 2017; Zhang et al. 2020a, b) Molecular simulations enable exploring the coupling mechanism of sorption and deformation at the molecular level. Kulasinski and colleagues built a molecular model of the secondary layer of wood cell wall, which is a bio-nanocomposite with CN reinforcing the soft amorphous matrix (Kulasinski et al. 2017). The molecular simulation could capture the anisotropy of the mechanical properties due to the presence of CN. Moisture content is found to be higher in the composite compared to the matrix and water molecules are found to cluster at the interface. This phenomenon was confirmed by Charlier and Mazeau, in a slightly different system which showed that the water molecules mainly remain in the volume adjacent to the interface (Charlier and Mazeau 2012). Despite these previous works, a better understanding of the impact of the presence of CN on the coupled behavior between the sorption and deformation of nanocomposites is required. Specifically, we will aim in the present paper at elucidating how CN influences the sorption-induced swelling of the composites and what role CN

plays in sorption and deformation hysteresis. To answer these questions, a molecular model of CN-reinforced cellulose composite, i.e., ACC (all-cellulose composite), is built to study the role of CN in the coupling between sorption and deformation of nanocomposites. The influence of CN on mechanical properties is first clarified, followed by a detailed study on the role of CN in sorption and sorption-induced deformation of the composite. Finally, the effect of the presence of CN on sorption and deformation hysteresis is also discussed.

2. Models and Methods

2.1. Molecular models

In this paper, we model a cellulose nanocrystal (CN) with 16 polymer chains, which corresponds to a crystal width about 2 nm. This is consistent with the experimental observations that CN is generally 2–20 nm wide (Habibi et al. 2010b). The 16 polymer chains are assembled to make an Iβ CN with the help of Cellulose-Builder (Figure 1(a)) (Gomes and Skaf 2012). Based on the atomic-resolution synchrotron and neutron diffraction data reported by Nishiyama et al (Nishiyama et al. 2002, 2003; Wada et al. 2004), Cellulose-Builder can generate Cartesian coordinates for all atoms of the specified structure in the Protein Data Bank format, suitable as starting configurations in molecular dynamics simulations and other calculations. Then the CN is imported into Material Studio 8.0 and positioned at the center of an orthogonal box. The remainder of the box volume is packed with amorphous cellulose (AC), which serves as the matrix of the composite. The resulting computational domain is used with periodic boundary conditions in all three directions in order to avoid finite size effect. For practical reason, the CN extends across the boundaries in the longitudinal direction (Kulasinski et al. 2017). In other words, CN is infinitely long with an infinitely large degree of

polymerization. This generally corresponds to a higher stiffness in the longitudinal direction compared to composites with finite sized reinforcements. In contrast, the degree of polymerization of AC is set to 20 cellubiose monomers. It has been verified in our precious work that AC with this 20 cellubiose monomers can reproduce the water sorption isotherms and mechanical properties measured on bulk AC (Chen et al. 2018). After the packing process, the raw configuration of the composite is subjected to a series of relaxation processes with the help of MD to obtain a well equilibrated stress-free configuration. Specifically, the composite is first relaxed in the *NVT* ensemble, which corresponds to a macroscopic system with constraints of constant number of particles (*N*), constant volume (*V*) and constant temperature (*T*), for 2 ns at a temperature T = 300 K. Then the composite is further relaxed in the *NPT* ensemble with constant number of particles, constant pressure P = 0 and constant temperature T = 300 K for 2 ns. To remove the possible residual stress generated in the packing process, the temperature is raised to 500 K and further relaxation is carried out in the *NPT* ensemble for 2 ns with P = 1 MPa to facilitate the matrix embracing the CN and also to increase the AC density. The CN is kept rigid at 500 K to prevent its amorphization. Then the external pressure is removed, and the temperature is reduced back to 300 K. As last step, the composite is relaxed in the NPT ensemble for 4 ns with pressure P = 0 and temperature T = 300 K. The final configuration of the composite after the relaxation process is shown in Figure 1(b). The volume fraction of CN is found to be 0.27 and the mass fraction 0.31. The density of AC is 1.35 $g.cm^{-3}$ and the density of the CN is 1.64 $g.cm^{-3}$. Both densities are comparable to experimental results of 1.48 $g.cm^{-3}$ (Chen et al. 2004) and 1.66 $g.cm^{-3}$ (Kulasinski et al. 2014) respectively. In dry state, the dimensions of the computational model are 5.4 × 4.4 × 4.2 nm^3. For water, we use the SPC/E water model. The interactions between atoms are modeled by PCFF

(Polymer Consistent Force Field) force field (Sun et al. 1994). Practically, the parameters of PCFF for different elements are directly imported from Material Studio 8.0. In our previous paper (Chen et al. 2018), we have showed the validity of combining PCFF and SPC/E in simulating water sorption in amorphous cellulose by comparing with the experimental sorption isotherms. With PCFF for amorphous cellulose and SPC/E for water, the simulation captured a lot of important features such as isotherm shape and sorption hysteresis. In this paper, we include a cellulose nanocrystal into the amorphous cellulose matrix, but the chemical composition is kept the same with amorphous cellulose. Thus, we continue to use the same force field parameters from our previous work (Chen et al. 2018).

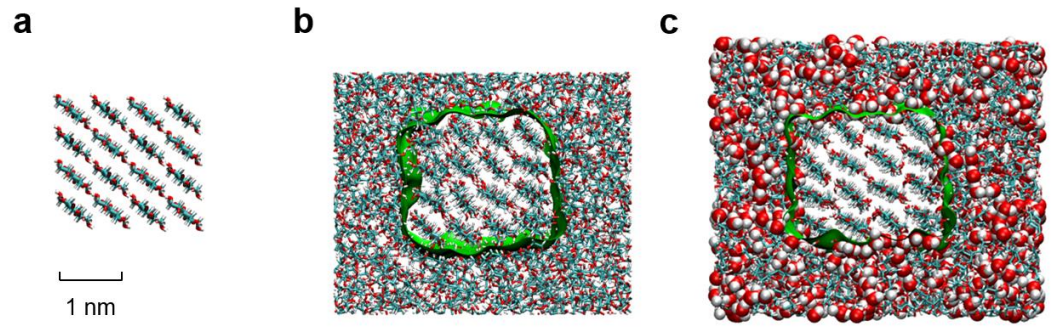

Figure 1. (a) Initial configuration of Iβ CN. **(b)** Configuration of the composite after relaxation process. The green surface is the surface of CN determined by Van der Waals radius. **(c)** Configuration of the composite with water molecules adsorbed into the matrix.

To characterize the role played by the CN in the hygromechanical behavior of the composite, three systems are built as schematically represented in Figure 2.

1. A bulk AC without CN. This system is used to characterize the sorption-deformation coupling in the pure AC matrix and serves as the reference when studying the role of CN.
2. A composite system with a CN in which the interaction between the CN and water is turned off. Technically, this can be achieved by turning off the electrostatic and Van der Waals interaction between CN and water. Note

that to prevent unphysical water diffusion into CN, the repulsive force between water and cellulose at very close distances (~0.2 nm in our case) is maintained on purpose. This means no preferential clustering of water molecules at the CN/matrix interface will occur, and only a mechanical reinforcing mechanism of CN is present. This system is termed as *partial-interaction* model as the direct impact of the CN on sorption is on purpose removed and only the CN-AC interaction is at play. By comparing results from the bulk AC and the *partial-interaction* model, the mechanical reinforcing role played by CN through CN-AC interactions can be characterized.

3. A composite with both CN-AC and CN-water interactions included. This system is termed as *full-interaction* model. In this last model, the presence of CN affects both AC and water clustering in the interface. Here the role of CN is not limited to mechanical reinforcement. Since CN shows hydrophilic surfaces, as there are plenty of hydroxyl groups exposed at its surfaces, the presence of CN in the composite has a direct impact on water sorption through the CN-water interaction. This effect can be examined by comparing the results of *partial-interaction* and *full-interaction* composites.

By investigating the behavior of these three systems, we characterize the role of CN with regard to sorption and mechanics respectively and the coupling between the two aspects.

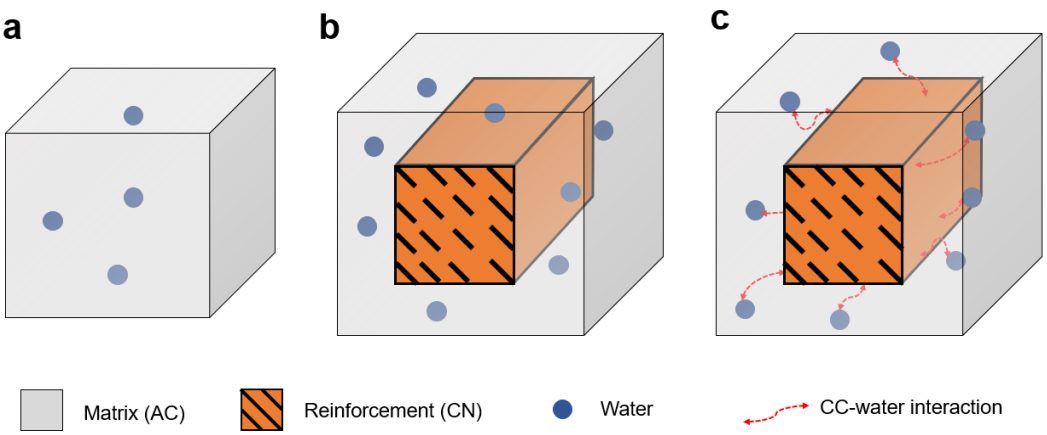

Figure 2. Three molecular models considered in this work: **(a)** bulk AC model without reinforcement of CN; **(b)** *partial-interaction* composite model with CN-water interactions turned off. **(c)** *full-interaction* composite model with CN-water interactions turned on.

2.2. Hybrid GCMC/MD simulation

To study the coupled effect between sorption and swelling, both aspects are modeled based on the osmotic ensemble ($\mu\sigma T$) which allows considering systems at constant temperature T, chemical potential μ, and stress σ. This ensemble permits to investigate water sorption while allowing for the deformation, or sorption-induced deformation (as well as moisture history and thus hysteresis). We perform simulations in this osmotic ensemble using a hybrid strategy that combines Grand Canonical Monte Carlo (GCMC) simulations with Isobaric-Isothermal MD simulations. One can refer to (Chen et al. 2018, 2019a) for a more detailed description of this hybrid technique. Specifically, at each chemical potential of interest, the free swelling of the composite is simulated using the hybrid GCMC/MD molecular simulations with $\sigma = 0$ and $T = 300$K. Each iteration consists of 2000 insertion/deletion MC attempts and 200 MD timesteps. The chemical potential is related to relative humidity RH according to $\mu - \mu_0 = k_B T \ln(RH)$, where μ_0 and k_B are chemical potential of water at saturation and Boltzmann constant. Adsorption and desorption are considered by varying the RH from 0 to 1.0 and from 1.0 back to 0 respectively. A snapshot of the configuration at saturation

(RH = 1.0) is displayed in Figure 1(c). It shows that water molecules are only adsorbed within the matrix - thus outside the CN - and that the composite undergoes significant swelling.

2.3. Characterization of hydrogen bonds

Cellulose is a non-crosslinked polymer so that hydrogen bonds are expected to play a crucial role in its cohesion and mechanical behavior. As shown in Figure 3 (a), a hydrogen bond is defined as a physical bond between an O and H atoms separated by a distance shorter than 0.35 nm and with an angle between the hydrogen donor and the acceptor smaller than 30˚. There are three types of hydrogen bonds as shown in Figure 3 (b, c, d): bonds formed between cellulose groups and other cellulose groups (HB^{PP}), bonds formed between water and cellulose groups (HB^{PW}) and bonds formed between water molecules and other water molecules (HB^{WW}). Specifically, HB^{PP} governs the inter-chain interaction and is thus crucial for the physical properties of cellulose. HB^{PW} indicates the interaction between cellulose chain and water molecules, i.e., the adsorbent-adsorbate interaction, thus can be utilized to identify water-molecules attached to the cellulose chains. HB^{WW} happens when RH is relatively high and a considerable number of water molecules has been adsorbed. In this paper, we mainly focus on polymer-related hydrogen bonds, i.e., HB^{PP} and HB^{PW}.

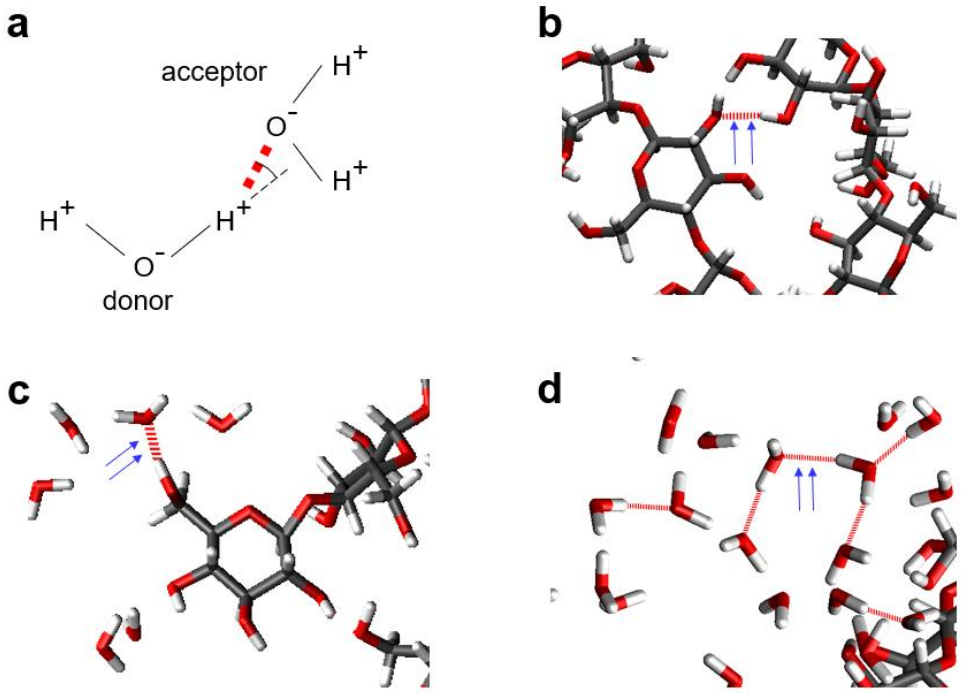

Figure 3 Hydrogen bonds identified in the water-cellulose system: **(a)** criterion is defined as distance shorter than 0.35 nm and angle smaller than 30°; **(b)** HB^{PP}: hydrogen bonds between cellulose and cellulose groups; **(c)** HB^{PW}: hydrogen bonds between cellulose groups and water molecules; **(d)** HB^{WW}: hydrogen bonds between water and water molecules.

2.4. Mechanical testing

Generally, a hydrated polymeric system shows significant dependence on moisture content regarding its mechanical properties. Here we mainly concentrate on the Young's modulus. The Young's modulus of the hydrated polymer in this paper is determined from the slope of the stress-strain relationship at small strains, i.e. in the linear/elastic regime. Tensile tests are performed at different moisture content in the *x*-, *y*- and *z*-directions respectively, where a linear uniaxial strain ranging from 0 to 0.05 is applied at constant temperature T = 300 K. The uniaxial strain is imposed by changing the corresponding dimension of the simulation box in the frame of a molecular dynamics run with a time span of 4 ns, while the pressure in the other two dimensions is set to zero using a Nose-Hoover barostat. The resulting tensile stress is extracted in a continuous fashion during the loading procedure to obtain the stress-strain curve. Note that loading is conducted at constant moisture content so that the measured quantity is the undrained Young's modulus.

2.5. Energy landscape

To examine the interaction between the CN and water molecules, we calculate the potential energy landscape of the CN regarding CN-water interaction. In this scenario, the influence of the AC matrix on water is omitted and only the CN-water interaction is taken into consideration. At the selected cross section, a 400×400 grid mesh is generated, upon which the potential energy is calculated at each grid point by placing a probe water molecule. Note that the probed potential energy depends on the orientation of water molecules. Thus, energy minimization is carried out at each grid point before extracting the potential energy.

3. Results and discussion

3.1 Role of CN on stiffness of ACC: reinforcing effect

First, we study the influence of CN on the stiffness of the material. The Young's modulus is determined by tensile tests in MD simulation (Chen et al. 2018) at certain moisture contents. As the bulk AC model is isotropic, the Young modulus is taken as the average of Young moduli for the three principle directions. For the *partial-interaction* and *full-interaction* composites, the presence of CN introduces a mechanical anisotropy into the system, and two Young's moduli are considered: one in the longitudinal direction E^{zz} and the other in the transverse direction E^{tt} (with the latter being calculated as the average of the moduli in x and y directions, i.e., $E^{tt}=(E^{xx} +E^{yy}) / 2$). The Young's moduli versus moisture content for the bulk AC, *partial-interaction* and *full-interaction* composites are compared in Figure 4. It shows that the two composites with/without CN-water interaction exhibit similar Young's moduli in both the longitudinal and transverse directions. This indicates that the CN influences the mechanical properties of the AC matrix mainly through the CN-AC interaction, while the role of CN-water interaction with regard to

mechanical behavior is less important. Therefore, with respect to the Young's moduli, we will not distinguish the two composite models but only the reinforcing effect.

Figure 4 shows that CN mainly reinforces the matrix in the longitudinal direction by a factor of about 8.0 compared with the bulk AC. On the other hand, the reinforcing effect in the transverse direction is limited to a factor of about 1.5. Besides, we find both the Young's modulus of buck AC and composite materials have strong dependence on the moisture content: Overall, the Young's modulus decreases against the moisture content, except at the low moisture content range, where the Young's modulus shows limited increase against the moisture content.

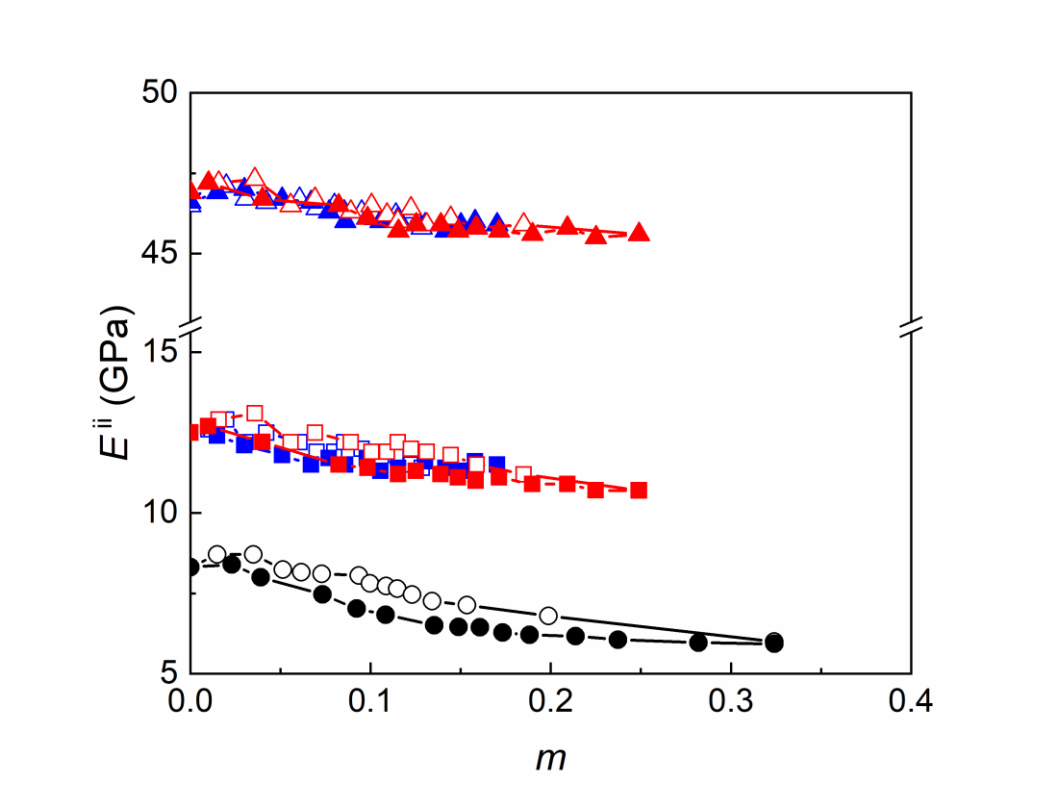

Figure 4. Relationship between Young modulus E and moisture content m. The black, blue and red circles dots represent the bulk AC, *partial-interaction* composite and *full-interaction* composite respectively. The open and closed symbols correspond to adsorption and desorption data. The circles, squares and triangles represent the Young modulus of the bulk AC, transverse Young modulus E^{tt} and longitudinal Young modulus E^{zz} , respectively.

297 The dependence of Young's modulus on moisture content for bulk polymers
298 and composites can be understood by studying the occurrence of hydrogen bonds in
299 the systems. Typically, there are three types of hydrogen bonds in a hydrated
300 polymer system: polymer-to-polymer hydrogen bonds HB^{PP}, polymer-to-water
301 hydrogen bonds HB^{PW} and water-to-water hydrogen bonds HB^{WW}, among which
302 HB^{PP} and HB^{PW} are particularly instructive about internal structural rearrangements
303 of polymer chains due to water sorption (Chen et al. 2018). Here we plot in Figure 5
304 the dependence of polymer related hydrogen bonds, i.e., HB^{PP} and HB^{PW} in the bulk
305 AC and in the matrix of the composites upon moisture content change. We can see
306 that HB^{PP} decreases against the moisture content for all three models while HB^{PW}
307 increases. This is mainly attributed to the swelling of AC upon water sorption. As
308 water gets adsorbed into the interchain space pushing away the neighboring
309 cellulose chains, the interchain distance increases and some HB^{PP} break, leading to
310 the mechanical weakening of the system. This explains the softening, or decrease of
311 Young's modulus, of the system upon water sorption.
312 Of interest, we also observe, in Figure 4, a mild increase of Young's modulus
313 at very low moisture content upon water sorption. Concurrently, we see in Figure 5
314 that the number of HB^{PP} barely decreases over this low moisture content range for
315 all three models. This indicates that most of the water molecules adsorbed at low
316 RH fill in the initially existing pores of the dry AC and only the water molecules
317 adsorbed afterwards result in more significant swelling of the polymer and breaking
318 of HB^{PP}. With the number of HB^{PP} almost constant and the configuration of AC
319 almost unaffected, the Young's modulus of the slightly hydrated system is higher
320 than the dry state as the initial porosity has been filled by the water molecules
321 without weakening the AC skeleton. This explains the mild increase of Young's
322 modulus versus moisture content at low RH shown by Figure 4.

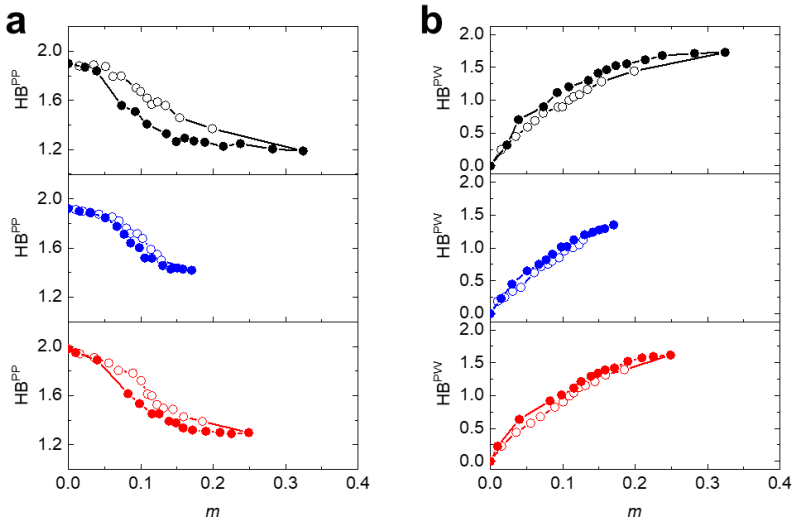

Figure 5 Dependence of number of (a) polymer-to-polymer hydrogen bonds (HB^{PP}) and (b) water-to-polymer hydrogen bonds (HB^{PW}) on moisture content. The results from three systems with bulk AC model, *partial-interaction* model and *full-interaction* model result in top (black), middle (blue) and bottom (red) panels, Adsorption and desorption results are plotted using open and closed circles respectively.

Now we consider the mechanical effect of adding CN reinforcement into the AC matrix. We find that, for the composite, the decrease in Young's modulus versus moisture content is more limited for transverse directions compared to the bulk AC (and even less for longitudinal direction). As the breaking of HB^{PP} relies on swelling of the AC matrix, a more limited swelling of AC due to the reinforcement of CN in the composite leads to fewer breakage of HB^{PP} (Figure 5), which finally results in less variation of Young modulus. Thus, we see less moisture content, less swelling, less breakage of HB^{PP} and less weakening effect at saturation.

Hysteresis in Young's modulus against moisture content is observed mainly for the bulk AC. A smaller hysteresis is observed for the transverse directions, while hysteresis for the longitudinal direction is very limited. The hysteresis in Young modulus arises from the hysteresis in HB^{PP}, which undergoes a different sequence along the adsorption and desorption branches. We can see clearly in Figure 5 (a) that there are more HB^{PP} in adsorption branch, which corresponds to higher Young's modulus compared to that in the desorption branch with the same moisture

content. i.e., the hysteretic modulus dependence on moisture content. The smaller hysteresis for the composites can be attributed to two major reasons: One is the less breaking of HB^{PP} due to less swelling caused by the reinforcing effect, which can be confirmed in Figure 5 (a) that there are more HB^{PP} left at saturation for the two composite models. The other is the mixing fact: Young's modulus of the composite is strongly affected by CN, which is a non-sorptive and mechanically reversible reinforcement. With the presence of CN, the mechanical properties of the composite are expected to be less hysteretic compared to that of the matrix.

3.2. Role of CN on the sorption and strain isotherms

Adsorption and desorption isotherms are plotted in Figure 6 (a). Moisture content m in the three cases is defined as $m = m^W/m^{AC}$, where m^W and m^{AC} are masses of water molecules and AC respectively. Generally, moisture content is defined as the ratio between the mass of water uptake and the total mass of composite. However, as water molecules are only adsorbed in the AC matrix, including its interface with CN, it is more insightful to exclude the mass of CN from the denominator. This definition allows us to directly compare the sorption behavior with/without CN.

The sorption isotherms of the three models are of type II according to the classification of IUPAC (International Union of Pure and Applied Chemistry) (Thommes et al. 2015). That is, the moisture content m increases sharply at low RH, slowly at medium RH range and then sharply again at large RH. Sorption hysteresis, which persists throughout the RH range from 0 to 1.0, is present in the three systems - although the size of the hysteresis loop differs. The sorption isotherms of the bulk AC model are compared to the experimental one (Mihranyan et al. 2004), with a shift of m= +0.05 to account for the presence of residual i.e., non-desorbable,

water due to experimental difficulties of attaining dry conditions or unavoidable partial rehydration upon weighing (Chen et al. 2018). The simulated sorption isotherms agree well with the experimental data.

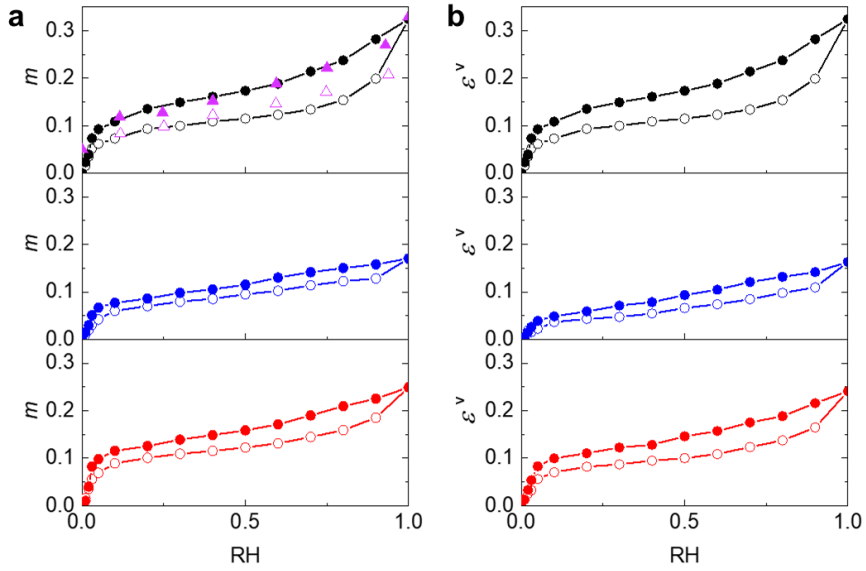

Figure 6. (a) Sorption isotherms and **(b)** Strain isotherms of the three systems with bulk AC model, *partial-interaction* model and *full-interaction* model results in top (black), middle (blue) and bottom (red) panels, at T = 300 K. Adsorption and desorption results from simulations are plotted using open and closed circles respectively. Experimental adsorption and desorption isotherms of pure AC are plotted using open and closed (purple) triangles (Mihranyan et al. 2004).

The strain isotherms of the three models are plotted in Figure 6 (b). By analogy with the definition of moisture content used above, the volumetric strain of AC is defined as $\varepsilon^V = \Delta V^{AC}/V_0^{AC}$, where V_0^{AC} and ΔV^{AC} are the initial and incremental volumes of AC matrix. The strain isotherms exhibit shapes similar to the ones of the sorption isotherms with a significant hysteresis. Both types of composites show a lower moisture content and swelling strain, indicating that the CN manifests its reinforcing effect not only in the modulus as discussed before but also in the sorption process. Moreover, the different sorption and strain isotherms of the *partial-interaction* and *full-interaction* composites demonstrate that the CN-water interaction also affects the results. These features indicate that CN plays

multiple roles in the sorption process which calls for additional characterization/investigation.

To study the reinforcing effect of CN on the sorption and swelling isotherms (i.e. versus RH), we plot the differential moisture content Δm and differential volumetric strain $\Delta\varepsilon^V$ (blue circles) in Figure 7 (a) between *partial-interaction* composite and bulk AC. These differences are defined as: $\Delta m = m|_{\text{partial}} - m|_{\text{AC}}$ and $\Delta\varepsilon^V = \varepsilon^V|_{\text{partial}} - \varepsilon^V|_{\text{AC}}$, where $m|_{\text{partial}}$, $\varepsilon^V|_{\text{partial}}$, $m|_{\text{AC}}$ and $\varepsilon^V|_{\text{AC}}$ are the moisture content and volumetric strain of the *partial-interaction* composite and bulk AC respectively. We see a significant reduction of the moisture content and volumetric strain, which can be attributed to the reinforcing effect of CN. As the swelling of matrix is constrained by the CN, there is less additional inter-chain space created in the matrix to accommodate water molecules. Thus, it becomes harder for water molecules to be adsorbed into the matrix at given RH and moisture content drops in the *partial-interaction* composite. As shown in Figure 7, the reduction of moisture content and of volumetric strain in desorption branches is greater than in the adsorption branches. This means that the sorption and strain hysteresis in the *partial-interaction* composite is compressed by the CN. We recall that, in the *partial-interaction* composite, the CN does not impose any direct impact on sorption as the CN-water interaction is turned off. We conclude that the reduction in moisture content in the *partial-interaction* composite, together with the compressed sorption hysteresis, is caused by the mechano-sorptive effect. This means that the sorption behavior is influenced by the mechanical conditions due to the coupling between sorption and deformation.

Apart from the reinforcing effect, CN is also expected to directly influence on the sorption process through the CN-water interaction. To study this effect, we plot the differential moisture content Δm and volumetric strain $\Delta\varepsilon^V$ between the *full* and

partial-interaction models in Figure 7. The differences are defined as: $\Delta m = m|_{full} - m|_{partial}$ and $\Delta\varepsilon^V = \varepsilon^V|_{full} - \varepsilon^V|_{partial}$ where $m|_{full}$ and $\varepsilon^V|_{full}$ are moisture content and volumetric strain of the *full-interaction* composite. Figure 7 shows that the difference values are positive (red circles), which means that the moisture content and the swelling become larger when the CN-water interaction is switched on. Moreover, this enhancement in sorption leads to larger sorption and deformation hysteresis. Because of the attraction of CN, more water molecules get adsorbed into the AC matrix, therefore inducing a larger swelling of the matrix (with more broken HB^{PP}). Thus, there are more hydroxyl groups on the polymer chains exposed as additional sorption sites for water molecules which finally contribute to the hysteresis of the system.

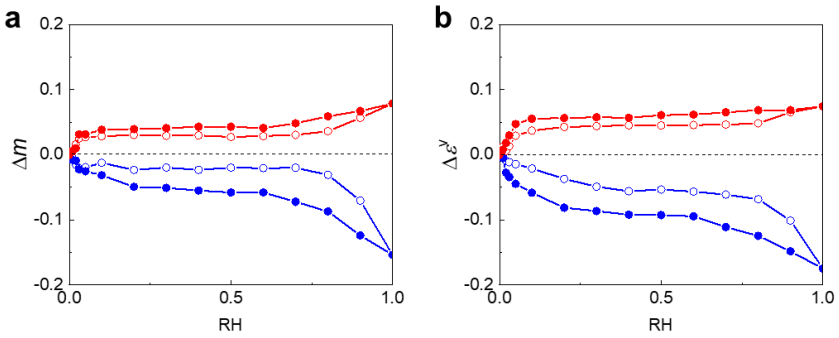

Figure 7. Differential **(a)** moisture content Δm and **(b)** volumetric strain $\Delta\varepsilon^V$ between the *partial-interaction* composite and AC (blue) and between the *full-interaction* composite and *partial-interaction* composite (red) as functions of RH. Open and closed circles represent adsorption and desorption respectively.

The difference of sorption and swelling between the two composites arises thus from the CN-water interaction. The strength of CN-water interaction can be characterized by looking at the energy landscape. As shown in Figure 8 (a), the potential energy within CN is positive, higher than 8.0 $kcal.mol^{-1}$. This means that

penetration of water molecules into the CN involves a large energy cost that is unlikely to happen. The energy landscape outside the CN corresponds to negative values, which means that water molecules minimize the system energy by approaching CN. Figure 8 (b) also shows that the most favorable adsorption sites are located at the concave surface, where the energy well is enhanced by the surrounding hydroxyl groups at the CN surface.

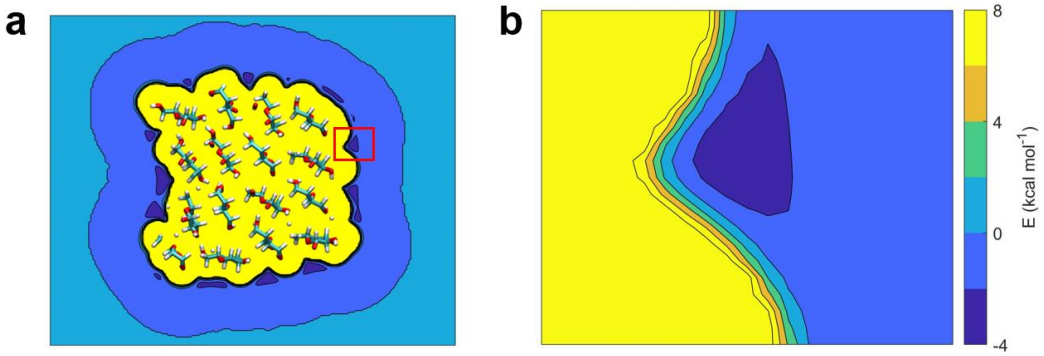

Figure 8. (a) Potential energy landscape of water molecules around the CN; **(b)** zoom-in of the energy landscape within the red box depicted in (a).

The direct influence of CN on sorption can also be probed by looking at water distributions in the matrix. Snapshots of water distribution in the *partial-interaction* and *full-interaction* composites at RH=1.0 are shown in Figure 9. The AC matrix is omitted in the plot. It shows that the water distributions in the matrix far enough from the CN are similar in the two cases. The main difference is seen at the CN/AC interface. For the *partial-interaction* composite, there is a very limited number of water molecules adsorbed at the interface, while water molecules tend to cluster at the interface for the *full-interaction* composite. This impression built on the snapshots is confirmed by checking water distributions within the slit formed between two CNs, which is displayed in the middle of Figure 9. The histogram of water distributions is acquired by averaging 2×10^6 MD timesteps upon sorption equilibrium at RH = 1.0. The data shown in Figure 9 are acquired over a black dashed box with dimensions 2.5 × 4.9 nm^2. It shows that there are very few water

molecules at the interface for the *partial-interaction* model and the moisture content increases gradually away from the interface until reaching a plateau. Though the plateau is not flat and the density profile is not symmetric because of the heterogeneous porous structure of AC matrix at such a finite size, we see that the interface exhibits a hydrophobic behavior. Moreover, the large stiffness of CN together with the CN-AC interaction makes the AC adjacent to CN stiffer and hard to swell, resulting in a reduction of the moisture content in the stiffened AC matrix region.

When turning to the *full-interaction* composite, this composite leads to water molecules clustering at the interface of the CN. The water density profile exhibits a peak at the interface. In this case, the CN-water interaction, as a competing factor against the reinforcing effect, comes into play. CN attracts water molecules to the interface and enhances water sorption. Though the reinforcing effect is still present and hinders water sorption, it shows in our case that the CN-water interaction is so strong at the interface that it dominates the sorption behavior there. In contrast, at the middle of the slit – i.e. far from the interface – both the reinforcing effect and the CN-water attraction diminish so that no significant difference in water distributions is found between the two cases. Similar enhanced water sorption at the reinforcement/matrix interface was reported previously by Kulasinski et al (Kulasinski et al. 2017), who attributed the enhanced sorption to the higher porous structure of the interface because of the structural mismatch between the reinforcement and matrix. However, considering that the mentioned structural mismatch and higher porous structure of the interface depend merely on the reinforcement/matrix interaction (which is the same for the *partial-interaction* and *full-interaction* composites), the explanation of a different interface structure does not hold. The comparison between the two different composites in this work reveals

that the enhanced water sorption at the interface is mainly due to the CN-water interaction rather than the microstructure of the interface due to structural mismatch.

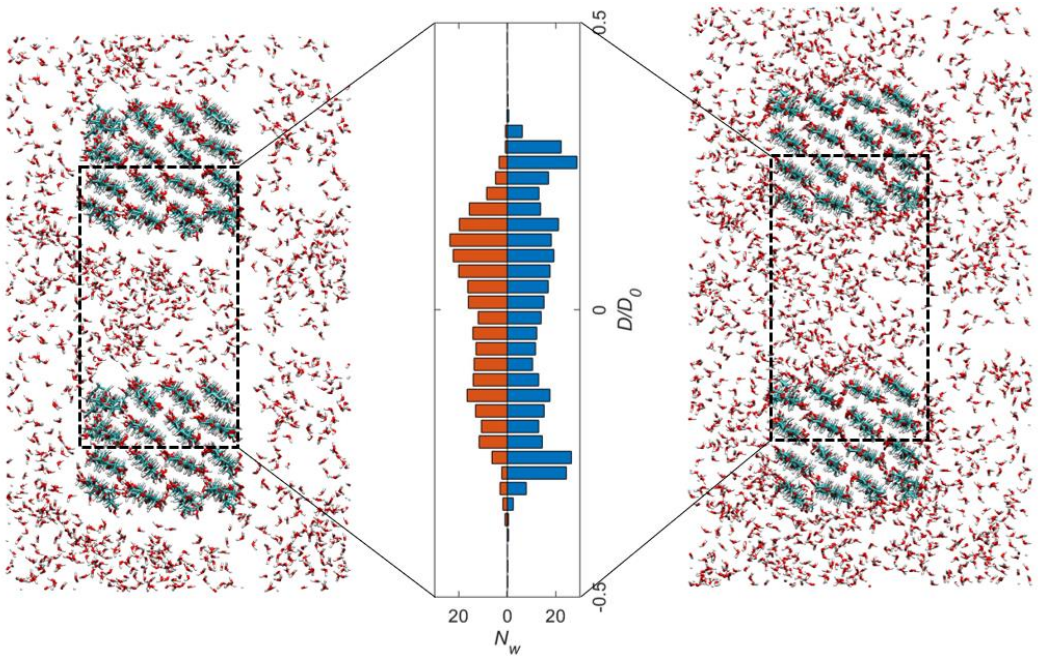

Figure 9. Typical molecular configurations of water molecules distributed in the matrix of *partial-interaction* (*left*) and *full-interaction* (*right*) composites projected along the longitudinal direction. The plot of matrix is omitted for better visualization of water distribution. The water density histograms within the black dashed boxes are plotted in the *middle*, with the red and blue data representing the *partial-interaction* and *full-interaction* composites respectively. D_0 = 4.9 nm is the length of the box.

Two competing mechanisms have been characterized so far in this subsection regarding the impact of CN on sorption and swelling behavior of the composites: the reinforcing effect of CN constrains the sorption and swelling, and the CN-water attraction enhances the sorption and swelling. The question naturally arises that what is the overall impact of CN on the sorption and swelling of the composite? For the current configuration studied in this paper, the overall effect of CN is constraining the sorption and swelling. This can be easily seen from Figure 6 by comparing the isotherms of bulk AC (top panel) and the full-interaction composite (bottom panel) as the magnitude of sorption/strain isotherm for the full-interaction composite is smaller than that for the bulk AC. This means that, for our

configuration, the constraining mechanism outperforms the enhancing mechanism. However, one must note the overall effect of CN should heavily depend on the composite configuration. One can expect that, with a different configuration (different volume fraction of CN, for instance), the enhancing mechanism may outperform the constraining mechanism, leading to an opposite overall effect compared to the configuration in this paper. As we mentioned in the Introduction, the overall effect of CN can be either enhancing or constraining according to experiments. The underlying reasons of this inconsistence between different experiments remain unknown. With the characterization of the enhancing and constraining mechanisms, we believe that this inconsistence could be explained by the competition of the two mechanisms.

3.3. Role of CN on swelling coefficients

In the adsorption/strains isotherms, lower/higher strains correspond to lower/higher moisture contents, indicating a monotonic relationship between moisture content and strain. This relationship is confirmed by plotting strain versus moisture content which shows a linear relationship with the moisture content for all the three systems, see Figure 10(a). Also, the data for adsorption and desorption collapse into a single relationship, meaning we get a unique $m \sim \varepsilon^{V}$ curve regardless of the presence of CN and the moisture history. In effect, water gets adsorbed into AC and creates the space for its accommodation by exerting repulsive forces on the polymer chains. This additional space created by the adsorbed water molecules is at the origin of the sorption-induced swelling. The same coupling physics persists throughout adsorption and desorption and remains the same in the different systems. As a result, all the data collapse on a single relationship on the $m \sim \varepsilon^{V}$ curve.

As CN introduces mechanical anisotropy into the composite, we check the uniaxial swelling behaviors of the three systems. Similar to the strategy used in our study of Young modulus, we define the uniaxial strain of bulk AC model as the average uniaxial strain of all three directions because of its isotropy. For the composites, we look at the longitudinal strain ε^{zz} and transverse strain ε^{tt} of the AC matrix, where ε^{tt} is calculated by the average of strain in two transverse directions, i.e., $\varepsilon^{tt} = (\varepsilon^{xx} + \varepsilon^{yy}) / 2$. The uniaxial strain of two composite systems are compared with the bulk AC in Figure 10(b). The uniaxial swelling coefficient is determined by the slope of the strain versus moisture content curve. It shows that there is no significant difference in the swelling coefficient for *partial-interaction* and *full-interaction* composites. Therefore, we only discuss in what follows the reinforcing effect and compare the uniaxial swelling coefficient of the bulk AC and the composites.

The swelling coefficients in the longitudinal and transverse directions of the composites are equal to 0.10 and 0.48. On the other hand, the swelling coefficient for bulk AC is 0.35. The small swelling coefficient in longitudinal direction of the composite compared to the bulk AC is attributed to the strong reinforcing effect of CN in the longitudinal direction. By contrast, the swelling coefficient of the composite in transverse direction is found to be higher than the uniaxial swelling coefficient of the bulk AC. We can explain this by the fact that the relationship between volumetric strain and moisture content is unique as the same moisture content leads to the same change of volume, thus the same volumetric strain. Since the swelling in the composite along the longitudinal direction is restrained by the reinforcing effect of CN, this strain will be much lower than 1/3 of the volumetric strain (which would be the case in an isotropic material). As a result, to obtain the same volumetric strain, the strain along the transverse directions will be higher than

1/3 of the volumetric strain, causing a swelling coefficient in transverse directions higher than that of bulk AC. We may conclude that the swelling coefficients, i.e. the amount of strain with increasing moisture content, only depends on the reinforcing effect as no difference between the two composites is seen.

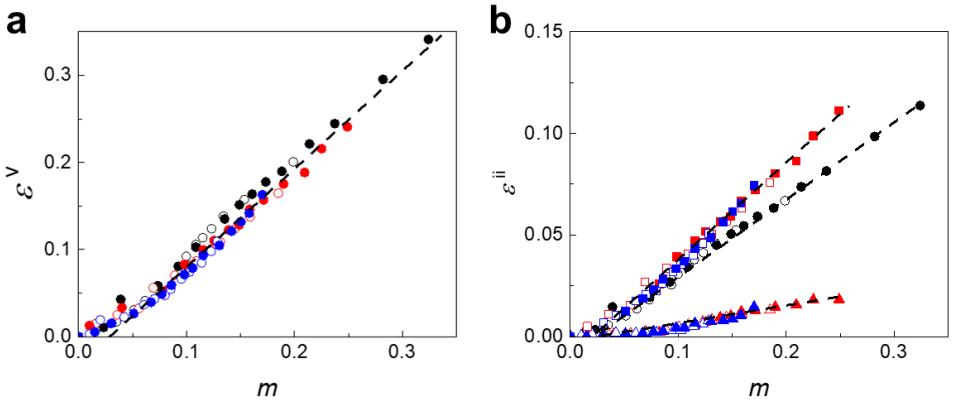

Figure 10. Relationship between **(a)** volumetric strain and **(b)** uniaxial strain and moisture content m. Black, blue and red circles represent the bulk AC, *partial-interaction* and *full-interaction* composites respectively. The open and closed symbols are the adsorption and desorption data. The circles, squares and triangles represent volumetric strain ε^V, transverse strain ε^{tt} and longitudinal strain ε^{zz} respectively. The black dashed lines are drawn as guides to the eye.

3.4. Influence of CN on hysteresis in sorption and swelling isotherms

Hysteresis is characterized by the difference of moisture content/strain between the desorption and adsorption branch, i.e., $H_{\text{moisture}}=m_{\text{de}} - m_{\text{ad}}$ and $H_{\text{strain}}=\varepsilon^V_{\text{de}} - \varepsilon^V_{\text{ad}}$, where m_{de}, m_{ad}, $\varepsilon^V_{\text{de}}$ and $\varepsilon^V_{\text{ad}}$ are moisture content and volumetric strain in the desorption and adsorption branch respectively. The sorption and strain hysteresis of the three systems are plotted in Figure 11. A comparison between the bulk AC (black circles) and *partial-interaction* composite (blue circles) clearly shows that the hysteresis shrinks because of the reinforcing effect of CN in both sorption and strain: H_{moisture} and H_{strain} are lower in the *partial-interaction* composite throughout

570 the entire RH range. According to (Chen et al. 2018), the hysteresis relies on the
571 breakage of HB^{PP} to expose the hydroxyl groups on polymer chains as additional
572 sorption sites for water molecules. The presence of CN constrains the deformation
573 of the AC matrix thus leading to less breakage of HB^{PP} as shown in Figure 5. As a
574 result, the hysteresis is greatly diminished by the mechanical reinforcing effect of
575 CN.

576 Comparison between the *partial-interaction* and *full-interaction* models shows
577 that hysteresis in both sorption and strain isotherms is enlarged by the CN-water
578 interaction. As discussed in Section 3.1, the CN-water interaction induces a
579 hydrophilic interface, where the sorption is greatly enhanced and results in a
580 clustering of water molecules. As a result, the AC matrix swells more to
581 accommodate the increased moisture content which leads to a larger number of
582 HB^{PP} breakage (Figure 5). This additional breakage of HB^{PP} finally contributes to
583 the enlarged sorption and deformation hysteresis. On the other hand, the hysteresis
584 of the *full-interaction* composite is smaller than that of the bulk AC, although larger
585 than the *partial-interaction* composite. This means that the reinforcing effect of CN
586 is more dominating for the current configure regarding hysteresis.

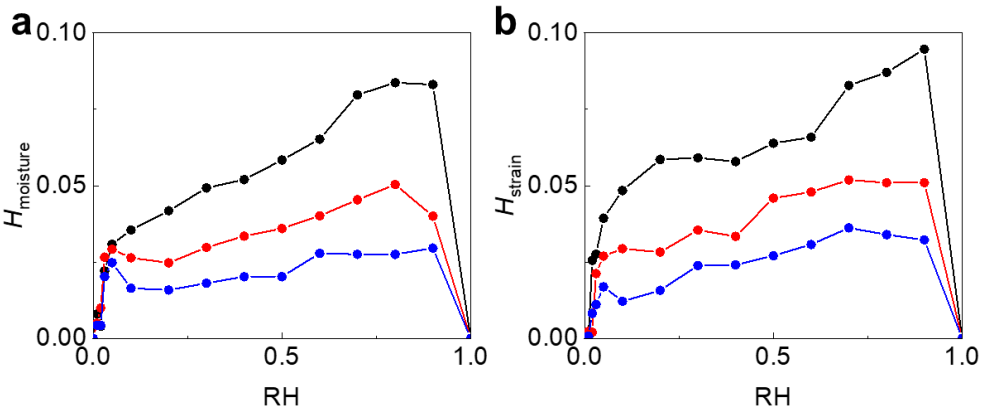

Figure 11. Hysteresis of three systems in **(a)** moisture content and **(b)** strain. The black, blue and red circles represent the bulk AC, *partial-interaction* composite and *full-interaction* composite respectively.

4. Conclusion

- This work addresses the role of cellulose nanocrystals (CN) in the coupling between sorption and deformation of CN-based nanocomposites and the related hysteresis phenomenon. With the help of hybrid GCMC/MD simulations, three samples are considered: pure amorphous cellulose (AC), CN/AC composite without CN-water interaction and CN/AC composite with CN-water interaction. By comparison between these different systems, we characterize the two major roles played by CN in the coupling behavior. One is the mechanical reinforcing effect through the CN-AC interaction, which stiffens the matrix and limits the swelling. As a result, water sorption in the AC matrix is hindered. Moreover, the sorption and strain hysteresis shrink because of the reduced breakage of hydrogen bonds due to the limited swelling. The other effect is the sorption enhancing effect through CN-water interaction, which attracts water toward the CN/AC

interface – which enhances sorption at the interface and increases the swelling. Accordingly, the hysteresis in both sorption and strain is enlarged due to sufficient hydrogen bond breaking. The sorption and swelling of the composite result from the competition of the two factors. Other aspects related to the two roles are also examined. We find anisotropic swelling and mechanical weakening behavior of the composite upon sorption because of the orientation of CN. Moreover, the mechanism of sorption at the CN/AC interface is characterized.

The findings presented in this work deepen our understanding of sorption and swelling of CN-reinforced nanocomposites and related hysteresis. The two competing roles of CN can be used for composite material design to tailor targeted coupled behaviors. More generally, as most works regarding the sorption-induced deformation in nonporous materials concentrate mainly on homogenous media, we expect that this work can bring attention to the sorption-induced deformation and related hysteresis of heterogenous nanocomposites which widely exist in nature.

Acknowledgements

The authors acknowledge the support of the Swiss National Science Foundation (SNSF) (no. 143601).

References

Anfara VA, Brown KM, Mangione TL (2002) Qualitative Analysis on Stage: Making the Research Process More Public. Educ Res 31:28–38. https://doi.org/10.3102/0013189X031007028

Anglès MN, Dufresne A (2001) Plasticized Starch/Tunicin Whiskers Nanocomposite Materials. 2. Mechanical Behavior. Macromolecules 34:2921–2931. https://doi.org/10.1021/ma001555h

631 Anglès MN, Dufresne A (2000) Plasticized Starch/Tunicin Whiskers
632 Nanocomposites. 1. Structural Analysis. Macromolecules 33:8344–8353.
633 https://doi.org/10.1021/ma0008701

634 Azizi Samir MAS, Alloin F, Sanchez J-Y, Dufresne A (2004) Cellulose
635 nanocrystals reinforced poly(oxyethylene). Polymer (Guildf) 45:4149–4157.
636 https://doi.org/10.1016/j.polymer.2004.03.094

637 Barkas WW (1939) Wood Water Relationships. IV. The Swelling and Shrinkage
638 of Wood in Relation to its Mechanical Properties. J Chem Inf Model 388.
639 https://doi.org/10.1017/CBO9781107415324.004

640 Blanco A, Monte MC, Campano C, et al (2018) Nanocellulose for Industrial Use.
641 In: Handbook of Nanomaterials for Industrial Applications. Elsevier, pp 74–
642 126

643 Brown RM (2004) Cellulose structure and biosynthesis: What is in store for the
644 21st century? J Polym Sci Part A Polym Chem 42:487–495.
645 https://doi.org/10.1002/pola.10877

646 Brown RM (1996) The Biosynthesis of Cellulose. J Macromol Sci Part A
647 33:1345–1373. https://doi.org/10.1080/10601329608014912

648 Charlier L, Mazeau K (2012) Molecular Modeling of the Structural and
649 Dynamical Properties of Secondary Plant Cell Walls: Influence of Lignin
650 Chemistry. J Phys Chem B 116:4163–4174.
651 https://doi.org/10.1021/jp300395k

652 Chen M, Coasne B, Derome D, Carmeliet J (2020) Coupling of sorption and
653 deformation in soft nanoporous polymers: Molecular simulation and
654 poromechanics. J Mech Phys Solids 137:103830.
655 https://doi.org/10.1016/j.jmps.2019.103830

656 Chen M, Coasne B, Guyer R, et al (2018) Role of hydrogen bonding in hysteresis
657 observed in sorption-induced swelling of soft nanoporous polymers. Nat
658 Commun 9:3507. https://doi.org/10.1038/s41467-018-05897-9

659 Chen M, Coasne B, Guyer R, et al (2019a) Molecular Simulation of Sorption-
660 Induced Deformation in Atomistic Nanoporous Materials. Langmuir
661 35:7751–7758. https://doi.org/10.1021/acs.langmuir.9b00859

662 Chen W, Lickfield GC, Yang CQ (2004) Molecular modeling of cellulose in
663 amorphous state. Part I: model building and plastic deformation study.
664 Polymer (Guildf) 45:1063–1071.
665 https://doi.org/10.1016/j.polymer.2003.11.020

666 Chen, Zhang, Shomali, et al (2019b) Wood–Moisture Relationships Studied with
667 Molecular Simulations: Methodological Guidelines. Forests 10:628.
668 https://doi.org/10.3390/f10080628

669 de Mesquita JP, Donnici CL, Teixeira IF, Pereira F V. (2012) Bio-based
670 nanocomposites obtained through covalent linkage between chitosan and

671 cellulose nanocrystals. Carbohydr Polym 90:210–217.
672 https://doi.org/10.1016/j.carbpol.2012.05.025

673 Derome D, Griffa M, Koebel M, Carmeliet J (2011) Hysteretic swelling of wood
674 at cellular scale probed by phase-contrast X-ray tomography. J Struct Biol
675 173:180–190. https://doi.org/10.1016/j.jsb.2010.08.011

676 Derome D, Rafsanjani A, Patera A, et al (2012) Hygromorphic behaviour of
677 cellular material: hysteretic swelling and shrinkage of wood probed by phase
678 contrast X-ray tomography. Philos Mag 92:3680–3698.
679 https://doi.org/10.1080/14786435.2012.715248

680 Favier V, Chanzy H, Cavaille JY (1995) Polymer Nanocomposites Reinforced by
681 Cellulose Whiskers. Macromolecules 28:6365–6367.
682 https://doi.org/10.1021/ma00122a053

683 Gomes TCF, Skaf MS (2012) Cellulose-Builder: A toolkit for building crystalline
684 structures of cellulose. J Comput Chem 33:1338–1346.
685 https://doi.org/10.1002/jcc.22959

686 Habibi Y, Goffin A-L, Schiltz N, et al (2008) Bionanocomposites based on
687 poly(ε-caprolactone)-grafted cellulose nanocrystals by ring-opening
688 polymerization. J Mater Chem 18:5002. https://doi.org/10.1039/b809212e

689 Habibi Y, Lucia LA, Rojas OJ (2010a) Cellulose Nanocrystals: Chemistry, Self-
690 Assembly, and Applications. Chem Rev 110:3479–3500.
691 https://doi.org/10.1021/cr900339w

692 Habibi Y, Lucia LA, Rojas OJ (2010b) Cellulose Nanocrystals: Chemistry, Self-
693 Assembly, and Applications. Chem Rev 110:3479–3500.
694 https://doi.org/10.1021/cr900339w

695 Hofstetter K, Hinterstoisser B, Salmén L (2006) Moisture uptake in native
696 cellulose – the roles of different hydrogen bonds: a dynamic FT-IR study
697 using Deuterium exchange. Cellulose 13:131–145.
698 https://doi.org/10.1007/s10570-006-9055-2

699 Huber T, Müssig J, Curnow O, et al (2012) A critical review of all-cellulose
700 composites. J Mater Sci 47:1171–1186. https://doi.org/10.1007/s10853-011-
701 5774-3

702 Kafy A, Akther A, Shishir MIR, et al (2016) Cellulose nanocrystal/graphene
703 oxide composite film as humidity sensor. Sensors Actuators A Phys
704 247:221–226. https://doi.org/10.1016/j.sna.2016.05.045

705 Karim Z, Mathew AP, Grahn M, et al (2014) Nanoporous membranes with
706 cellulose nanocrystals as functional entity in chitosan: Removal of dyes from
707 water. Carbohydr Polym 112:668–676.
708 https://doi.org/10.1016/j.carbpol.2014.06.048

709 Kulasinski K, Derome D, Carmeliet J (2017) Impact of hydration on the
710 micromechanical properties of the polymer composite structure of wood

711 investigated with atomistic simulations. J Mech Phys Solids 103:221–235.
712 https://doi.org/10.1016/j.jmps.2017.03.016

713 Kulasinski K, Keten S, Churakov S V., et al (2014) A comparative molecular
714 dynamics study of crystalline, paracrystalline and amorphous states of
715 cellulose. Cellulose 21:1103–1116. https://doi.org/10.1007/s10570-014-
716 0213-7

717 Kulasinski K, Salmén L, Derome D, Carmeliet J (2016) Moisture adsorption of
718 glucomannan and xylan hemicelluloses. Cellulose 23:1629–1637.
719 https://doi.org/10.1007/s10570-016-0944-8

720 Liu C, Jin R-N, Ouyang X, Wang Y-G (2017) Adsorption behavior of
721 carboxylated cellulose nanocrystal—polyethyleneimine composite for
722 removal of Cr(VI) ions. Appl Surf Sci 408:77–87.
723 https://doi.org/10.1016/j.apsusc.2017.02.265

724 Luzar A, Chandler D (1993) Structure and hydrogen bond dynamics of water–
725 dimethyl sulfoxide mixtures by computer simulations. J Chem Phys
726 98:8160–8173. https://doi.org/10.1063/1.464521

727 Luzar A, Chandler D (1996) Hydrogen-bond kinetics in liquid water. Nature
728 379:55–57. https://doi.org/10.1038/379055a0

729 Maréchal Y, Chanzy H (2000) The hydrogen bond network in I β cellulose as
730 observed by infrared spectrometry. J Mol Struct 523:183–196.
731 https://doi.org/10.1016/S0022-2860(99)00389-0

732 Mariano M, El Kissi N, Dufresne A (2014) Cellulose nanocrystals and related
733 nanocomposites: Review of some properties and challenges. J Polym Sci Part
734 B Polym Phys 52:791–806. https://doi.org/10.1002/polb.23490

735 Mazeau K, Charlier L (2012) The molecular basis of the adsorption of xylans on
736 cellulose surface. Cellulose 19:337–349. https://doi.org/10.1007/s10570-011-
737 9643-7

738 Mihranyan A, Llagostera AP, Karmhag R, et al (2004) Moisture sorption by
739 cellulose powders of varying crystallinity. Int J Pharm 269:433–442.
740 https://doi.org/10.1016/j.ijpharm.2003.09.030

741 Nishino T, Matsuda I, Hirao K (2004) All-Cellulose Composite. Macromolecules
742 37:7683–7687. https://doi.org/10.1021/ma049300h

743 Nishiyama Y, Langan P, Chanzy H (2002) Crystal structure and hydrogen-
744 bonding system in cellulose Iβ from synchrotron X-ray and neutron fiber
745 diffraction. J Am Chem Soc 124:9074–9082.
746 https://doi.org/10.1021/ja0257319

747 Nishiyama Y, Sugiyama J, Chanzy H, Langan P (2003) Crystal Structure and
748 Hydrogen Bonding System in Cellulose Iα from Synchrotron X-ray and
749 Neutron Fiber Diffraction. J Am Chem Soc 125:14300–14306.
750 https://doi.org/10.1021/ja037055w

751 Patera A, Derluyn H, Derome D, Carmeliet J (2016) Influence of sorption
752 hysteresis on moisture transport in wood. Wood Sci Technol 50:259–283.
753 https://doi.org/10.1007/s00226-015-0786-9

754 Patera A, Derome D, Griffa M, Carmeliet J (2013) Hysteresis in swelling and in
755 sorption of wood tissue. J Struct Biol 182:226–234.
756 https://doi.org/10.1016/j.jsb.2013.03.003

757 Qi H, Cai J, Zhang L, Kuga S (2009) Properties of Films Composed of Cellulose
758 Nanowhiskers and a Cellulose Matrix Regenerated from Alkali/Urea
759 Solution. Biomacromolecules 10:1597–1602.
760 https://doi.org/10.1021/bm9001975

761 Rafieian F, Jonoobi M, Yu Q (2019) A novel nanocomposite membrane
762 containing modified cellulose nanocrystals for copper ion removal and dye
763 adsorption from water. Cellulose 26:3359–3373.
764 https://doi.org/10.1007/s10570-019-02320-4

765 Safari S, van de Ven TGM (2016) Effect of Water Vapor Adsorption on Electrical
766 Properties of Carbon Nanotube/Nanocrystalline Cellulose Composites. ACS
767 Appl Mater Interfaces 8:9483–9489. https://doi.org/10.1021/acsami.6b02374

768 Salmén L (2004) Micromechanical understanding of the cell-wall structure. C R
769 Biol 327:873–880. https://doi.org/10.1016/j.crvi.2004.03.010

770 Sánchez-García MD, Hilliou L, Lagarón JM (2010) Morphology and Water
771 Barrier Properties of Nanobiocomposites of κ/ι-Hybrid Carrageenan and
772 Cellulose Nanowhiskers. J Agric Food Chem 58:12847–12857.
773 https://doi.org/10.1021/jf102764e

774 Sanchez-Garcia MD, Lagaron JM (2010) On the use of plant cellulose
775 nanowhiskers to enhance the barrier properties of polylactic acid. Cellulose
776 17:987–1004. https://doi.org/10.1007/s10570-010-9430-x

777 Sun H, Mumby SJ, Maple JR, Hagler AT (1994) An ab Initio CFF93 All-Atom
778 Force Field for Polycarbonates. J Am Chem Soc 116:2978–2987.
779 https://doi.org/10.1021/ja00086a030

780 Taylor DM (2002) Direct Cortical Control of 3D Neuroprosthetic Devices.
781 Science (80-) 296:1829–1832. https://doi.org/10.1126/science.1070291

782 Thommes M, Kaneko K, Neimark A V., et al (2015) Physisorption of gases, with
783 special reference to the evaluation of surface area and pore size distribution
784 (IUPAC Technical Report). Pure Appl Chem 87:1051–1069.
785 https://doi.org/10.1515/pac-2014-1117

786 Wada M, Chanzy H, Nishiyama Y, Langan P (2004) Cellulose III I crystal
787 structure and hydrogen bonding by synchrotron X-ray and neutron fiber
788 diffraction. Macromolecules 37:8548–8555.
789 https://doi.org/10.1021/ma0485585

790 Williamson RE, Burn JE, Hocart CH (2002) Towards the mechanism of cellulose
791 synthesis. Trends Plant Sci 7:461–467. https://doi.org/10.1016/S1360-
792 1385(02)02335-X

793 Yu X, Tong S, Ge M, et al (2013) Adsorption of heavy metal ions from aqueous
794 solution by carboxylated cellulose nanocrystals. J Environ Sci 25:933–943.
795 https://doi.org/10.1016/S1001-0742(12)60145-4

796 Zhang C, Coasne B, Guyer R, et al (2020a) Moisture-induced crossover in the
797 thermodynamic and mechanical response of hydrophilic biopolymer.
798 Cellulose 27:89–99. https://doi.org/10.1007/s10570-019-02808-z

799 Zhang C, Shomali A, Guyer R, et al (2020b) Disentangling Heat and Moisture
800 Effects on Biopolymer Mechanics. Macromolecules 53:1527–1535.
801 https://doi.org/10.1021/acs.macromol.9b01988

802